In situ high-temperature powder X-ray diffraction study on the spinel solid solutions $(Mg_{1-x}Mn_x)Cr_2O_4$

Sicheng Wang, Xi Liu, Yingwei Fei, Qiang He & Hejing Wang

Physics and Chemistry of Minerals

ISSN 0342-1791
Volume 39
Number 3

Phys Chem Minerals (2012) 39:189-198
DOI 10.1007/s00269-011-0474-8

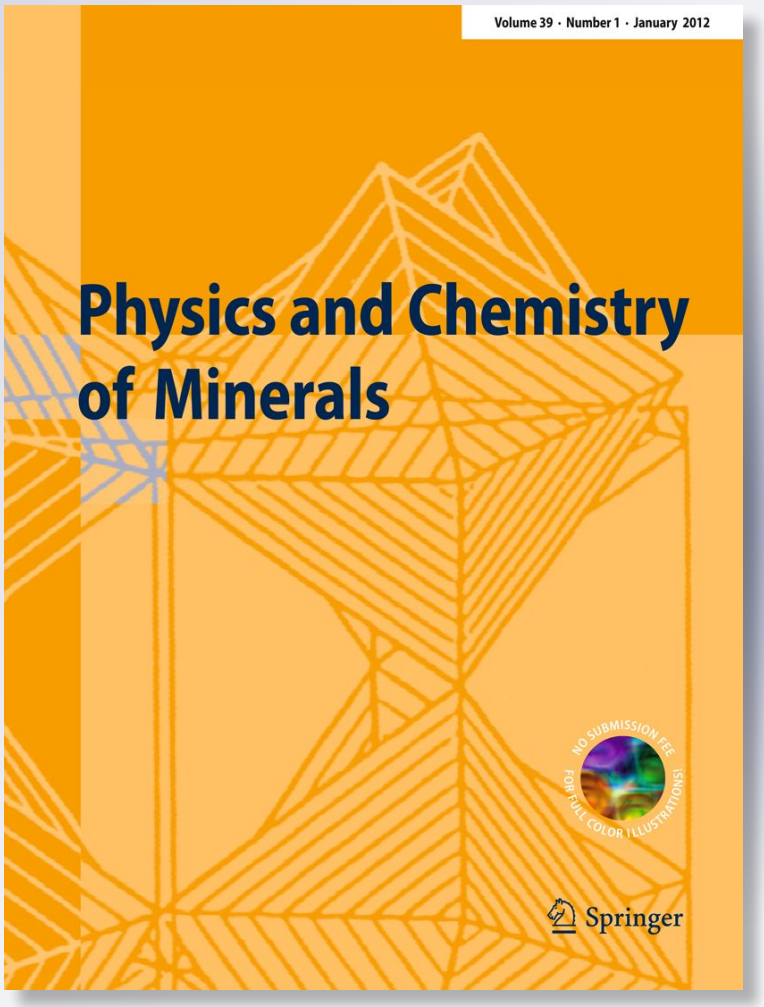

Springer

Phys Chem Minerals (2012) 39:189–198
DOI 10.1007/s00269-011-0474-8

ORIGINAL PAPER

In situ high-temperature powder X-ray diffraction study on the spinel solid solutions $(Mg_{1-x}Mn_x)Cr_2O_4$

Sicheng Wang · Xi Liu · Yingwei Fei · Qiang He · Hejing Wang

Received: 8 October 2011 / Accepted: 5 December 2011 / Published online: 18 December 2011

Abstract Using a conventional high-T furnace, the solid solutions between magnesiochromite and manganochromite, $(Mg_{1-x}Mn_x)Cr_2O_4$ with $x = 0.00, 0.19, 0.44, 0.61, 0.77$ and 1.00, were synthesized at 1,473 K for 48 h in open air. The ambient powder X-ray diffraction data suggest that the V–x relationship of the spinels does not show significant deviation from the Vegard's law. In situ high-T powder X-ray diffraction measurements were taken up to 1,273 K at ambient pressure. For the investigated temperature range, the unit-cell parameters of the spinels increase smoothly with temperature increment, indicating no sign of cation redistribution between the tetrahedral and octahedral sites. The V–T data were fitted with a polynomial expression for the volumetric thermal expansion coefficient ($\alpha_T = a_0 + a_1T + a_2T^{-2}$), which yielded insignificant a_2 values. The effect of the composition on a_0 is adequately described by the equation $a_0 = [17.7(8) - 2.4(1) \times x]\ 10^{-6}\ K^{-1}$, whereas that on a_1 by the equation $a_1 = [8.6(9) + 2.1(11) \times x]\ 10^{-9}\ K^{-2}$.

Keywords Cation redistribution · High-T X-ray diffraction · $(Mg_{1-x}Mn_x)Cr_2O_4$ · Thermal expansion · Spinel solid solutions

S. Wang · X. Liu (✉) · Y. Fei · Q. He · H. Wang
The Key Laboratory of Orogenic Belts and Crustal Evolution, Ministry of Education of China, Beijing 100871, China
e-mail: xi.liu@pku.edu.cn

S. Wang · X. Liu · Y. Fei · Q. He · H. Wang
School of Earth and Space Sciences, Peking University, Beijing 100871, China

Y. Fei
Geophysical Laboratory, Carnegie Institution of Washington, 5251 Broad Branch Road, NW, Washington, DC 20015, USA

Introduction

Spinels appear in various geological settings and have important geological implications. Chromian spinels ubiquitously occur in basalts and peridotites and are used as "petrologic litmus paper" being extremely sensitive to host rock petrogenesis (Dick and Bullen 1984). Spinel with the composition Mg_2SiO_4 (ringwoodite) is the most abundant phase in the deep transition zone of the Earth's mantle and has been observed in the Tenham chondritic meteorite (Binns et al. 1969). In some rare cases, spinels can occur as mineral inclusions in quartz in metamorphosed sediments which were probably subducted to depths >350 km and quickly returned to the surface of the Earth (Liu et al. 2007). Recently, spinels were found to be highly concentrated in some lunar rocks or lunar meteorites, potentially reflecting some aspects of the magma's evolution history of the Moon (Pieters et al. 2011; Gross and Treiman 2011).

Presumably due to their importance in the Earth sciences, the structure of spinels has been extensively investigated both by experimentation and by thermodynamic modeling (Hill et al. 1979; O'Neill and Navrotsky 1983, 1984; Della Giusta and Ottonello 1993; O'Neill and Dollase 1994; Jung 2006). Recently, first-principles simulation method was employed to study the physical–chemical features of spinels as well (Catti et al. 1999; Moriwake et al. 2002). Spinels have the general formula AB_2O_4, usually either A being a divalent and B trivalent cation (the so-called 2–3 spinels), or A being a quadrivalent and B a divalent cation (the so-called 4–2 spinels). In most cases, spinels have the space group $Fd\bar{3}m$, in which the oxygens present as a cubic close packing array, and A and B cations occupy one-eighth of the tetrahedral (8a) and half of the octahedral (16d) sites, respectively. As temperature increases, however, the A and

B cations of the spinels might become crystallographically disordered, and the general chemical formula then becomes $[A_{(1-i)}B_i]^{tet}[A_iB_{(2-i)}]^{oct}O_4$. If i, the inversion parameter, equals 0 or 1, the spinel has an ordered normal or inverse cation distribution ($[A]^{tet}[B_2]^{oct}O_4$, normal spinel; $[B]^{tet}[AB]^{oct}O_4$, inverse spinel); if $i = 2/3$, apparently, the A and B cations are randomly distributed between the tetrahedral and octahedral sites.

Extensive cation substitution can take place on both the tetrahedrally coordinated site and the octahedrally coordinated site, leading to a wide range of spinel solid solutions such as those of $MgCr_2O_4$–$FeCr_2O_4$ (Lenaz et al. 2004), $MgCr_2O_4$–$MgFe_2O_4$ (Lenaz et al. 2006) and $MgAl_2O_4$–$MgCr_2O_4$ (Klemme and Ahrens 2007). Synthetic pure $MgCr_2O_4$ spinel (magnesiochromite) and $MnCr_2O_4$ spinel (manganochromite) have been known for a long time and extensively investigated (e.g. Hastings and Corliss 1962; Raccah et al. 1966; Freyria Fava et al. 1997; Catti et al. 1999; Moriwake et al. 2002; Song et al. 2003; Gilewicz-Wolter et al. 2005; Stefan and Irvine 2011). Due to the large excess octahedral crystal field stabilization energy of Cr^{3+} (O'Neill and Navrotsky 1984), Cr-bearing spinels, specifically magnesiochromite and manganochromite here, should be 2–3 normal spinels. Indeed, experimental investigations and ab initio simulations of magnesiochromite and manganochromite have demonstrated their normal cation distribution (Hastings and Corliss 1962; Raccah et al. 1966; Freyria Fava et al. 1997; Catti et al. 1999; Moriwake et al. 2002; Stefan and Irvine 2011). With Mg^{2+} and Mn^{2+} replacing each other on the tetrahedral sites, the possibility of a 2–3 normal spinel solid solution series of the composition $(Mg_{1-x}Mn_x)Cr_2O_4$ is very high, as suggested by the field observation (Paraskevopoulos and Economou 1981). So far this possibility has not been experimentally evaluated yet, which explains why Park et al. (2009) had to assume an ideal solid solution model for this potential spinel solid solution series in their thermodynamic calculation. In the present study, we experimentally investigated whether there exists a complete solid solution series between $MgCr_2O_4$ and $MnCr_2O_4$ and how, if it exists, this solid solution series behaves at both room and high temperatures.

Experiment

The targeted compositions of the synthetic spinels along the $MgCr_2O_4$–$MnCr_2O_4$ join were $(Mg_{1-x}Mn_x)Cr_2O_4$ with $x = 0.0$, 0.2, 0.4, 0.6, 0.8 and 1.0. Chemicals MgO (99.9%), Cr_2O_3 (99.9%) and $MnCO_3$ (99.9%) were used to prepare the starting materials. Before being weighed, the oxides were dried at 1,073 K for 24 h, whereas $MnCO_3$ was kept at 373 K for 48 h in a drying oven (Biernacki and Pokrzywnicki 1999), in order to remove moisture absorbed by the chemicals from air. The chemicals were then weighed in appropriate proportions corresponding to the targeted spinel compositions, ground and homogenized manually in an agate mortar under acetone and pressed into pellets. Subsequently, these pellets were placed in platinum crucibles and sintered with a high-temperature furnace in open air. The samples were heated at 1,473 K for 48 h and slowly cooled to room temperature at the rate of −5 K/min. The sintered pellets changed their colors from light green to dark green with increasing Mn content. Part of each pellet was crushed into fine powder for later high-T X-ray diffraction experiments, and another part of the pellet was mounted in epoxy and polished using a series of diamond pastes for later SEM characterization and compositional analysis.

Both Cr and Mn are transition elements and can have multiple charge states, so that oxygen fugacity is potentially a very important factor for the successful synthesizing of the spinel solid solutions $(Mg_{1-x}Mn_x)Cr_2O_4$. Lucky enough, both magnesiochromite (Stefan and Irvine 2011) and manganochromite (Raccah et al. 1966; Song et al. 2003; Gilewicz-Wolter et al. 2005) were previously synthesized successfully at high temperatures in open air. On the other hand, O'Neill and Dollase (1994) claimed that a small amount of Cr^{4+} might present the $MgCr_2O_4$ spinel when its synthesizing atmosphere was open air. With the compositional and XRD data shown later, we tend to believe that our synthesizing of the spinel solid solutions $(Mg_{1-x}Mn_x)Cr_2O_4$ was successful, with nearly all Mn cations as Mn^{2+} and nearly all Cr cations as Cr^{3+}.

We examined the synthetic spinels by using optical microscopy, scanning electron microscopy (Quanta 200 FEG), transmission electron microscope (H9000NAR), powder X-ray diffraction (XRD; X'Pert Pro MPD system) and Zeiss AURIGA CrossBeam FIB/FESEM (Focused Ion Beam combined with Field Emission Scanning Electron Microscope) system. The high-resolution 300 kV transmission electron microscope (School of Physics, Peking University) guaranteed a resolution of 1 Å (crystal lattice) or 1.8 Å (point to point), so that the micromorphology of the fine synthetic spinels could be clearly visualized. Quantitative chemical composition analyses were made by using the state-of-the-art Zeiss AURIGA CrossBeam FIB/FESEM system at the Geophysical Laboratory, Carnegie Institution of Washington. The instrument was equipped with an Oxford X-Max large area (80 mm^2) analytical EDX SDD (Silicon Drift Detector), which provided much lower electronic noise and high count-rate over traditional Si(Li) and Ge solid-state detectors. The use of SDD allowed accurate determination of chemical compositions with energy-dispersive X-ray spectroscopy (EDX). The equipment was calibrated with the standards of enstatite,

forsterite, chromite and spessartine. The analyses were done at 15 kV, with a spatial resolution of about 600 nm, which was apparently small enough for our tiny spinel grains.

The high-T powder X-ray diffraction experiments at ambient pressure were conducted by using the X'Pert Pro MPD system attached with an Anton Paar HTK-1200 N oven capable to achieve 1,473 K with an accuracy of ±2 K (Hu et al. 2011). The heating oven was controlled by a Eurotherm temperature controller (Eurotherm 2604; type S thermocouple checked against the melting point of NaCl). Other details of the X'Pert Pro MPD system were a Cu target, operation voltage of 40 kV and current of 40 mA, as detailed in our previous studies (Hu et al. 2011; He et al. 2011; Liu et al. 2012). High-T experiments were conducted up to 1,273 K. At each desired temperature, data collection of the powder diffraction spectrum was initialized after that temperature was reached and the sample was allowed to thermally relax for 5 min. X-ray data were collected between 10 and 80°2θ, with a scanning step width of 0.017°2θ and a counting time of 10 s for each scanning step. Once the data collection was completed at that temperature, the experimental temperature was raised to the next target with a ramp of 10 K/min. The alignment of the X-ray diffractometer system was checked with the standard of a silicon crystalline powder at ambient temperature only. As the experimental temperature increased, the furnace and sample holder components and the powder sample itself expanded, which led to a small sample displacement. By adopting the data-processing procedure verified in Hu et al. (2011), the influence of this small sample displacement was readily corrected by a full powder X-ray pattern refinement using the MDI's program Jade 5.0 (Material Data, Inc.), and unit-cell parameters with high accuracy were successfully obtained.

Result and discussion

Our electron back-scatter images (not shown here) suggested that all synthesizing experiments resulted in two phases, with the dominant phase identified as spinel and the trace phase identified as unreacted eskolaite by ambient powder X-ray diffraction data. This observation is well in line with the experimental investigation of O'Neill and Dollase (1994). Our high-resolution TEM image showed that most spinel grains were octahedral or pseudo-octahedral, with their sizes ranging from ~0.5 to 1.5 μm (Fig. 1). The powder X-ray diffraction data collected at ambient temperature revealed that all major peaks could be assigned to the spinel structure, with the exception of a few weak peaks most likely originating from the trace amounts of eskolaite (Fig. 2). Considering the relative intensities of the X-ray diffraction peaks from these two phases, the unreacted eskolaite should be negligible, and the actual compositions of the spinels should closely match their initial designs. The composition data listed in Table 1 verify this expectation. Anyhow, the presence of negligible amounts of unreacted eskolaite and the absence of corresponding amounts of MgO and/or MnO in the synthetic experimental products suggested that the Cr_2O_3 content in the spinels should be more or less lower than required by the targeted chemical formulas of the spinels, which is positively confirmed by the data in Table 1 (about 3 mol%

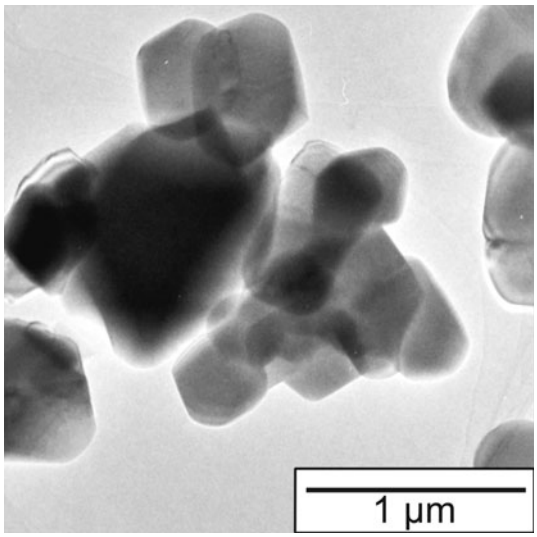

Fig. 1 High-resolution TEM image showing the micromorphology of the synthetic spinels (Sample WL000)

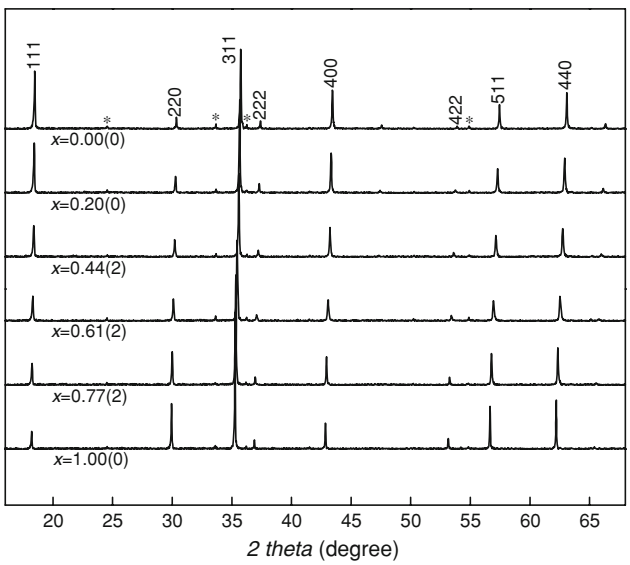

Fig. 2 XRD patterns of the spinel solid solutions $(Mg_{1-x}Mn_x)Cr_2O_4$ at room temperature. All major peaks can be assigned to spinel, whereas some small peaks as indicated by the *asterisks* can be assigned to eskolaite

Table 1 Composition of spinel solid solutions $(Mg_{1-x}Mn_x)Cr_2O_4$

Sample #	WL000(4)[a]	WL002(4)	WL004(5)	WL006(5)	WL008(4)	WL010(3)
MgO	20.87(65)[b]	16.73(51)	11.18(39)	7.92(40)	4.33(34)	–
MnO	–	7.10(6)	15.25(21)	21.92(24)	25.99(27)	32.33(8)
Cr_2O_3	79.13(66)	76.18(50)	73.57(38)	69.92(43)	69.68(20)	67.67(8)
Total	100.00	100.01	100.00	99.76	100.00	100.00
Cations per 4 oxygens						
Mg	1.00(3)	0.82(2)	0.57(2)	0.42(2)	0.23(2)	–
Mn	–	0.20(0)	0.44(1)	0.66(1)	0.79(1)	1.02(0)
Cr	2.00(3)	1.99(2)	1.99(1)	1.95(1)	1.98(1)	1.99(0)
Total	3.00(1)	3.01(1)	3.00(1)	3.02(1)	3.01(0)	3.01(0)
x[c]	0.00(0)	0.20(0)	0.44(2)	0.61(2)	0.77(2)	1.00(0)

[a] Number in the parentheses after the sample # indicates the number of quantitative analyses performed with the Zeiss AURIGA CrossBeam FIB/FESEM system

[b] Number in the parentheses represents one standard deviation in the rightmost digit (wt%)

[c] $x = Mn/(Mg + Mn)$

in maximum). Presumably, a small amount of Cr cation in the spinels might present as Cr^{4+} (O'Neill and Dollase 1994); alternately, there might be a small amount of Cr vacancy in the spinel structure (Moriwake et al. 2002). Nevertheless, the effect of this potential Cr^{4+} or Cr vacancy is unimportant due to its small quantity.

Mixing behavior

The unit-cell parameters of the pure end-members magnesiochromite ($a = 8.3364(1)$ Å) and manganochromite ($a = 8.4393(1)$ Å) determined in this study are much comparable to the literature data. For the magnesiochromite, the previously reported values were $a = 8.3340$ Å (O'Neill and Dollase 1994) and $a = 8.3364(4)$ Å (Stefan and Irvine 2011). For the manganochromite, the previously reported values were $a = 8.437(2)$ Å (Hastings and Corliss 1962) and $a = 8.437$ Å (Raccah et al. 1966).

The unit-cell parameters of the $(Mg_{1-x}Mn_x)Cr_2O_4$ spinel solid solutions are shown in Fig. 3. Considering the size similarity of the Mg^{2+} and Mn^{2+} in the fourfold coordination (0.57 and 0.66 Å, respectively; Shannon 1976), the substitution between Mg^{2+} and Mn^{2+} might not significantly change the unit cell. Indeed, the unit-cell parameter a expands only by about 1.2%, and the unit-cell parameter V expands by about 3.8% with a full replacement of Mg^{2+} by Mn^{2+} (Table 2). As shown in Fig. 3, the Vegard's law (linear relationship) generally holds for the present solid solution series. In detail, the small deviation from the Vegard's law is extremely small for the spinels with $x < 0.2$, and discernibly positive for the spinels with $x > 0.2$, resulting in the weak "S" shape of the unit-cell parameter-composition curve.

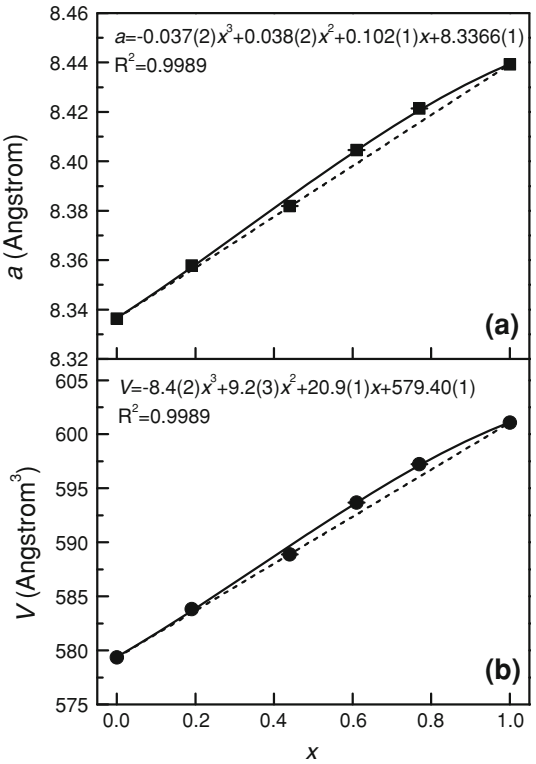

Fig. 3 Effect of composition on the unit-cell parameters of the spinel solid solutions $(Mg_{1-x}Mn_x)Cr_2O_4$ at room temperature: **a** the axis a; **b** the volume V

The nearly ideal mixing along the $MgCr_2O_4$–$MnCr_2O_4$ join should be expected, since both Mg^{2+} and Mn^{2+} are similar in size and since both magnesiochromite and manganochromite are 2–3 normal spinels and share similar charge distributions and cation arrangements. Other 2–3 normal spinel solid solutions such as $CoRh_2O_4$-$ZnRh_2O_4$ (Fiorani and Viticoli 1980), $CoAl_2O_4$–$MgAl_2O_4$ (Rosén

Table 2 Unit-cell parameters of spinel solid solutions $(Mg_{1-x}Mn_x)Cr_2O_4$

T (K)	$x = 0.00$[a]		$x = 0.20$		$x = 0.44$		$x = 0.61$		$x = 0.77$		$x = 1.00$	
	a (Å)	V (Å^3)	a (Å)	V (Å^3)	a (Å)	V (Å^3)	a (Å)	V (Å^3)	a (Å)	V (Å^3)	a (Å)	V (Å^3)
300	8.3364(1)[b]	579.34(1)	8.3579(1)	583.83(1)	8.3819(2)	588.87(2)	8.4046(2)	593.68(2)	8.4214(1)	597.24(1)	8.4393(1)	601.07(1)
373	8.3394(1)	579.96(1)	8.3616(1)	584.61(1)	8.3843(3)	589.39(4)	8.4088(1)	594.57(1)	8.4249(2)	597.99(2)	8.4436(1)	601.99(2)
473	8.3461(1)	581.37(1)	8.3666(2)	585.65(2)	8.3894(3)	590.46(3)	8.4148(2)	595.84(2)	8.4304(1)	599.15(1)	8.4493(1)	603.19(1)
573	8.3528(1)	582.77(1)	8.3735(1)	587.11(1)	8.3974(1)	592.16(2)	8.4208(2)	597.13(3)	8.4358(1)	600.31(2)	8.4545(1)	604.32(1)
673	8.3586(1)	583.99(1)	8.3792(2)	588.31(1)	8.4020(1)	593.14(2)	8.4261(2)	598.25(2)	8.4428(1)	601.82(2)	8.4608(1)	605.67(1)
773	8.3652(2)	585.36(1)	8.3877(2)	590.09(1)	8.4099(3)	594.80(3)	8.4329(1)	599.69(1)	8.4501(1)	603.37(1)	8.4676(1)	607.13(1)
873	8.3719(1)	586.78(1)	8.3941(2)	591.47(2)	8.4172(1)	596.34(2)	8.4395(1)	601.10(1)	8.4570(1)	604.84(1)	8.4744(1)	608.59(1)
973	8.3789(1)	588.25(1)	8.4011(1)	592.93(2)	8.4253(2)	598.07(2)	8.4476(1)	602.84(1)	8.4638(2)	606.31(2)	8.4815(1)	610.13(1)
1,073	8.3871(2)	589.98(2)	8.4088(1)	594.56(1)	8.4300(1)	599.08(2)	8.4543(1)	604.28(1)	8.4714(1)	607.94(1)	8.4889(1)	611.72(1)
1,173	8.3943(1)	591.50(1)	8.4150(1)	595.89(1)	8.4387(2)	600.92(2)	8.4628(1)	606.09(1)	8.4779(1)	609.35(1)	8.4967(1)	613.42(1)
1,273	8.4026(2)	593.26(2)	8.4229(1)	597.56(1)	8.4462(1)	602.54(1)	8.4697(2)	607.59(2)	8.4862(5)	611.15(7)	8.5045(1)	615.11(1)

[a] x is defined as Mn/(Mg + Mn), as in Table 1

[b] Number in the parentheses represents one standard deviation in the rightmost digit

and Muan 1966), $CoAl_2O_4$–$MnAl_2O_4$ (Jacob and Fitzner 1977), $CoCr_2O_4$–$MnCr_2O_4$ (Jacob and Fitzner 1977), $FeAl_2O_4$–$MgAl_2O_4$ (Jacob and Patil 1998) and $FeCr_2O_4$–$MgCr_2O_4$ (Lenaz et al. 2004) also show nearly perfect ideal mixing. It should be emphasized, however, that the compositions of the spinels in the early investigations, a key factor in evaluating the behavior of any solid solution series, were determined by mass balance rather than by modern direct quantitative analysis.

Thermal expansivity

In situ high-T powder diffraction experiments on the spinel solid solutions $(Mg_{1-x}Mn_x)Cr_2O_4$ were conducted up to 1,273 K and did not show any signal of phase transition. Figure 4 displays some typical XRD patterns collected on sample WL006 at different temperatures. The unit-cell parameters derived from the XRD patterns are listed in Table 2 and shown in Fig. 5. Apparent in Fig. 5 is the smooth variation of the unit-cell parameters with the temperature increment for all investigated samples, suggesting that no significant cation redistribution took place between the tetrahedral and octahedral sites of the spinels. For some spinels of different compositions (e.g. $MgAl_2O_4$, Suzuki and Kumazawa 1980; Co_3O_4, Liu and Prewitt 1990; $FeAl_2O_4$, Harrison et al. 1998; $MgFe_2O_4$, Levy et al. 2004), it was observed that the trends between the unit-cell parameters and temperatures changed their slopes at about 873–1,073 K, indicating the activation of cation diffusion and reordering between the tetrahedral and octahedral sites. Presumably due to the large excess octahedral crystal field stabilization energy of Cr^{3+} ($\Delta CFSE_{(oct-tet)}$ is about

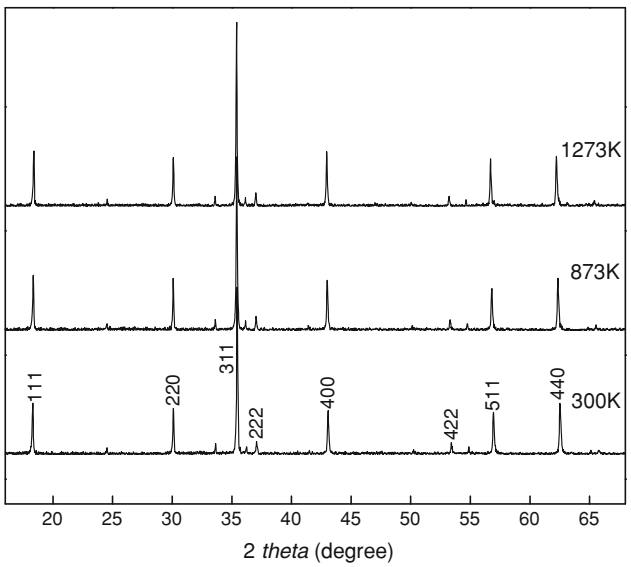

Fig. 4 Typical XRD patterns of the spinel solid solutions $(Mg_{1-x}Mn_x)Cr_2O_4$ at high temperatures (Sample WL006 randomly selected)

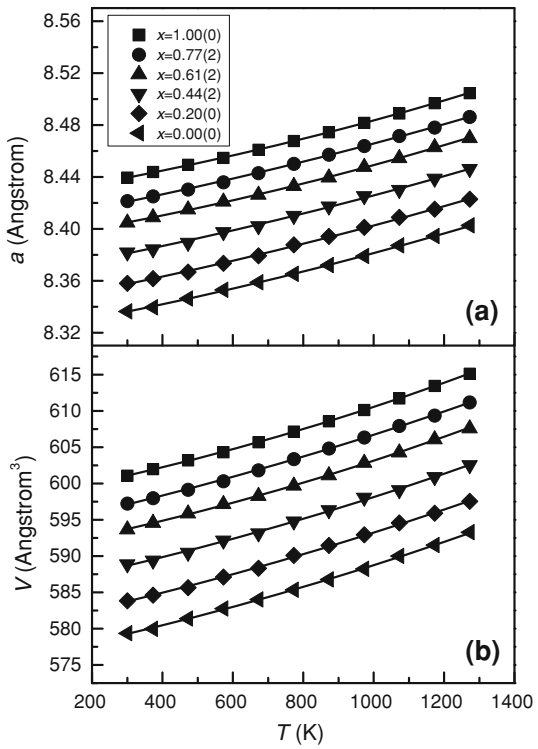

Fig. 5 Evolution of unit-cell parameters a and V of the spinel solid solutions $(Mg_{1-x}Mn_x)Cr_2O_4$ with temperature. *Curves* are drawn to guide the eye

−160 kJ/mol; O'Neill and Navrotsky 1984), our spinels maintained their 2–3 normal cation distribution in the investigated temperature interval and did not become more disordered as temperature increased. For the $MgCr_2O_4$ spinel, O'Neill and Dollase (1994) experimentally demonstrated no cation redistribution up to its melting temperature. No similar experimental work has been done with the $MnCr_2O_4$ spinel, but it is well expected that the Mn^{2+} cations should have less chance than the Mg^{2+} cations to enter the octahedral sites: the necessary energy input for their placement into the octahedral sites is −0(4) kJ/mol, compared with the required energy input of −25.1 kJ/mol for the placement of the Mg^{2+} cations (Kovtunenko 1997).

The volume-temperature data have been fitted to the following equations,

$$V_T = V_0 \exp\left[\int_0^T \alpha_T dT\right]$$

and

$$\alpha_T = a_0 + a_1 T + a_2 T^{-2},$$

where V_T, V_0 and α_T, are the high-T volume, room-T volume and volumetric thermal expansion coefficient at temperature T, respectively. a_0, a_1 and a_2 are the constants obtained in fitting the experimental V-T data. Replacing the volume data in the equations above with the axial dimension, the axial thermal expansion coefficients can be obtained similarly. We have found that the a_2 term is insignificant in both cases. The so-derived values for our six samples are listed in Table 3 and shown in Fig. 6. In general, the replacement of Mg by Mn in the spinel solid solutions $(Mg_{1-x}Mn_x)Cr_2O_4$ decreases a_0 but increases a_1, both for the volume and for the a-axis. Specifically, the effects of the composition on the values of a_0 and a_1 are $a_0 = [17.7(8) - 2.4(1) \times x]\ 10^{-6}\ K^{-1}$ and $a_1 = [8.6(9) + 2.1(11) \times x]\ 10^{-9}\ K^{-2}$ for the volumetric thermal expansion coefficients and $a_0 = [5.9(3) - 0.8(1) \times x]\ 10^{-6}\ K^{-1}$ and $a_1 = [2.8(3) + 0.7(4) \times x]\ 10^{-9}\ K^{-2}$ for the a-axial thermal expansion coefficients (Fig. 6).

It follows that, at ambient temperature (∼298 K), the $MgCr_2O_4$ spinel has a larger thermal expansion coefficient than that of the $MnCr_2O_4$ spinel (Table 4). Since a material with a larger thermal expansivity usually has a larger compressibility (smaller bulk modulus), this result is generally in line with the theoretic work done by Catti et al. (1999), which demonstrated that the bulk modulus of the $MgCr_2O_4$ spinel was slightly smaller than that of the $MnCr_2O_4$ spinel.

Thermal expansivity of various spinels at 298 K

The thermal expansion coefficients of our spinels along the join $MgCr_2O_4$–$MnCr_2O_4$ are compared to the earlier measurements in Table 4. Considering the potential differences in the investigated materials, experimental techniques and data-processing procedures used in the different investigations, the agreement among all these studies is excellent. The thermal expansion coefficients of the $MgCr_2O_4$ spinel and $MnCr_2O_4$ spinel determined by Qu et al. (2006) and Stefan and Irvine (2011) appear slightly larger than other measurements, simply because they are

Table 3 Parameters of the thermal expansion coefficients $(\alpha = a_0 + a_1 \times T)$ of spinel solid solutions $(Mg_{1-x}Mn_x)Cr_2O_4$

Composition of spinel	a-Axis		Volume	
	a_0^a	a_1^b	a_0^a	a_1^b
$MgCr_2O_4$	5.7(3)[c]	3.1(4)	17.1(9)	9.3(11)
$(Mg_{0.82}Mn_{0.20})Cr_2O_4$	6.3(5)	2.3(6)	18.8(15)	7.0(19)
$(Mg_{0.57}Mn_{0.44})Cr_2O_4$	5.8(7)	2.9(9)	17.3(21)	8.6(27)
$(Mg_{0.42}Mn_{0.66})Cr_2O_4$	5.3(3)	3.4(4)	15.9(10)	10.2(12)
$(Mg_{0.23}Mn_{0.79})Cr_2O_4$	5.7(4)	2.9(5)	17.0(11)	8.8(14)
$MnCr_2O_4$	5.1(1)	3.6(2)	15.2(4)	10.8(5)

[a] $\times 10^{-6}\ K^{-1}$

[b] $\times 10^{-9}\ K^{-2}$

[c] Number in the parentheses represents one standard deviation in the rightmost digit

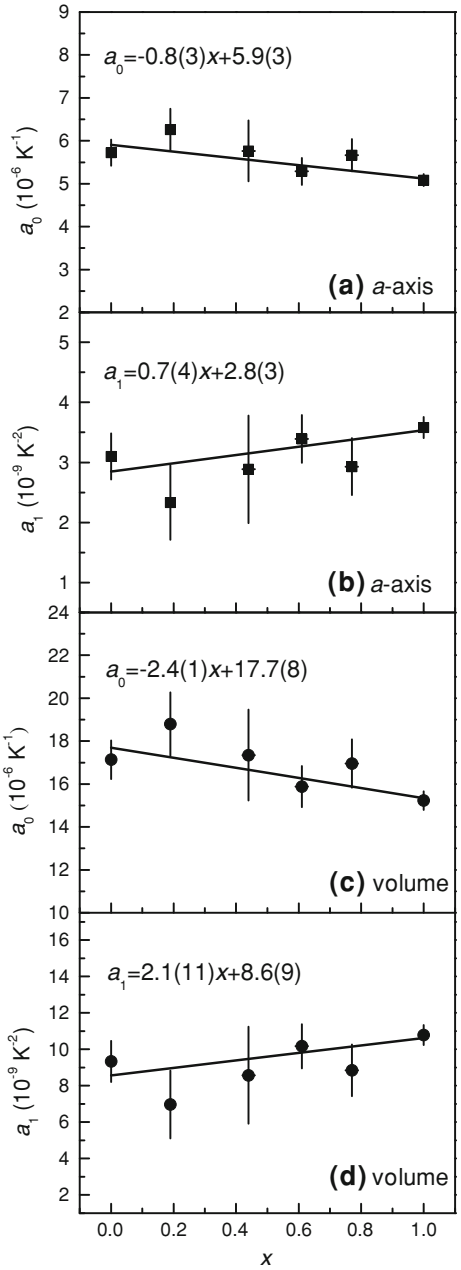

Fig. 6 Effect of composition on the thermal expansion coefficients of the spinel solid solutions $(Mg_{1-x}Mn_x)Cr_2O_4$: **a** a_0 and **b** a_1 for the a-axis and **c** a_0 and **d** a_1 for the volume

averaged values for wide temperature intervals, from 298 to 1,173 K and from 373 to 1,173 K, respectively.

The thermal expansion coefficients of these 2–3 normal spinels along the join $MgCr_2O_4$–$MnCr_2O_4$ are compared with those of other spinels with Cr cations fully occupying the octahedral sites in Table 4. Since the Cr cations strongly prefer the octahedral sites, all other cations have to occupy the tetrahedral sites. This cation distribution pattern is so effective that even temperature does not have any effect on it, as demonstrated with the $MgCr_2O_4$ spinel by O'Neill and Dollase (1994). Being so, the factors that can affect the accuracy of the thermal expansivity determination are thus very few, and the interpretation of the experimental results is rather straightforward. Table 4 clearly suggests that the thermal expansion coefficients of all those spinels with Cr cations on their octahedral sites, but one, are similar in magnitude, considering the variation of the cation sizes of Ni (0.55 Å), Mg (0.57 Å), Co (0.58 Å), Zn (0.60 Å) and Mn (0.66 Å) on the tetrahedral sites (Shannon 1976). This is a remarkable result in good agreement with our experimental observation made in this study. The thermal expansion coefficient of the $FeCr_2O_4$ spinel appears odd (Skinner 1966; Fei 1995), and further experimental investigation is necessary.

For other 2–3 oxide spinels listed in Table 4, it is difficult to evaluate the quality of the data due to some additional contributing factors such as the difference in the order–disorder states and the difference in the investigated temperature intervals. Although a critical evaluation of the data is out of the scope of this study, it is appropriate to point out that some discrepancies do exist, which is vividly exampled by the $MgAl_2O_4$ spinel (Yamanaka and Takéuchi 1983; Grimes and Al-Ajaj 1992). At low temperatures, this spinel has a normal structure. As temperature increases to about 873–973 K (Yamanaka and Takéuchi 1983), however, it starts to become disordered, which means the activation of the cation exchange between the octahedral and tetrahedral sites. The redistribution of the cations over these two kinds of sites then leads to some variation in the thermal expansion coefficients, as predicted by Hazen and Yang (1999). However, the prediction does not closely meet the experimental determination of the thermal expansion coefficients. According to Hazen and Yang (1999), the predicted thermal expansion coefficient for the normal structure is large, about 27.6×10^{-6} K^{-1}, whereas that for the inverse structure is small, about 24.0×10^{-6} K^{-1}. In contrast, the experimentally determined values are in an opposite order (from 17.67 at low temperature to 24.9 and then 29.4×10^{-6} K^{-1} at high temperature; Grimes and Al-Ajaj 1992; Yamanaka and Takéuchi 1983; Table 4). It is believed that at least some part of this conflict rooted in the experimental investigations, in which materials with different residual cation disorder states quenched from different annealing temperatures were used (O'Neill and Navrotsky 1983; Harrison et al. 1998; Hazen and Yang 1999). The preservation of the cation order–disorder state during the quenching process is apparently a complicate function of composition, annealing temperature, annealing time and quenching rate, which was unfortunately not thoroughly examined in most experimental studies.

The available thermal expansion coefficients of some 4–2 oxide spinels, including ringwoodite, are also compared

Table 4 Thermal expansion coefficients of different spinels at 298 K

Spinel composition	$\alpha(\times 10^{-6}\ K^{-1})$	Data source
2–3 spinel along the $MgCr_2O_4$–$MnCr_2O_4$ join		
$MgCr_2O_4$	18.24	Stefan and Irvine (2011)[a]
$MgCr_2O_4$	16.5	Fei (1995)[b]
$MgCr_2O_4$	17.1(9)	This study
$(Mg_{0.82}Mn_{0.20})Cr_2O_4$	18.8(15)	This study
$(Mg_{0.57}Mn_{0.44})Cr_2O_4$	17.3(21)	This study
$(Mg_{0.42}Mn_{0.66})Cr_2O_4$	15.9(10)	This study
$(Mg_{0.23}Mn_{0.79})Cr_2O_4$	17.0(11)	This study
$MnCr_2O_4$	15.2(4)	This study
$MnCr_2O_4$	22.41	Stefan and Irvine (2011)[a]
$MnCr_2O_4$	21.6	Qu et al. (2006)[c]
Other 2–3 oxide spinels		
$NiCr_2O_4$	22.8	Qu et al. (2006)[c]
$CoCr_2O_4$	22.2	Qu et al. (2006)[c]
$ZnCr_2O_4$	23.0(4)	Levy et al. (2005)
$FeCr_2O_4$	9.9	Fei (1995)[b]
$ZnAl_2O_4$	20.43	Levy and Artioli (1998)
$Zn[Al_{0.5}Fe_{0.5}]_2O_4$	21.18	Levy and Artioli (1998)
$ZnFe_2O_4$	19.29	Levy and Artioli (1998)
$MgAl_2O_4$	17.67	Grimes and Al-Ajaj (1992)[d]
$MgAl_2O_4$	24.9	Yamanaka and Takéuchi (1983)[e]
$MgAl_2O_4$	29.4	Yamanaka and Takéuchi (1983)[f]
$Mg[Al_{0.4}Cr_{0.6}]_2O_4$	19.92	Levy and Artioli (1998)
$FeAl_2O_4$	15.6	Fei (1995)[b]
$FeAl_2O_4$	21.9	Harrison et al. (1998)[g]
$MgFe_2O_4$	20.5	Fei (1995)[b]
$MgFe_2O_4$	27.3	Levy et al. (2004)
Co_3O_4	14.8	Liu and Prewitt (1990)[h]
Fe_3O_4	20.6	Fei (1995)[b]
Some 2–4 oxide spinels		
Mg_2GeO_4	32.1	Ross and Navrotsky (1987)[h]
Mg_2SiO_4	30.7(6)	Inoue et al. (2004)
Mg_2TiO_4	24.6(4)	O'Neill et al. (2003)[i]
Fe_2SiO_4	51(25)	Yamanaka (1986)[j]
Ni_2SiO_4	35(3)	Yamanaka (1986)[j]

Only the thermal expansion coefficients at 298 K compared, with some being *T*-independent, whereas others being *T*-dependent

[a] Result obtained by using a NETZSCH Dilatometer 402C

[b] Data compiled by Fei (1995) from an earlier compilation (Skinner 1966)

[c] Result obtained by using a SETARAM Scientific Industrial Setsys16/18 multifunction thermal analysis device

[d] Result derived from the low-*T* measurements from 77 to 300 K

[e] Normal spinel analyzed in the temperature range of 293–873 K; data reprocessed by Fei (1995)

[f] Disordered spinel analyzed in the temperature range of 993–1,933 K; data reprocessed by Fei (1995)

[g] Data reprocessed by our method, yielding $a_0 = 21.9(9) \times 10^{-6}\ K^{-1}$, $a_1 = 7.7(8) \times 10^{-9}\ K^{-2}$ and $a_2 = -0.5(1)$ K

[h] Data reprocessed by Fei (1995)

[i] Data of the first series of experiments reprocessed by our method, yielding $a_0 = 24.6(4) \times 10^{-6}\ K^{-1}$ and $a_1 = 10.8(5) \times 10^{-9}\ K^{-2}$

[j] Data reprocessed by Smyth et al. (2000)

in Table 4. Apparently, the 4–2 oxide spinels, in general, have larger thermal expansion coefficients than 2–3 oxide spinels.

Acknowledgments We thank Professor J. Chen for her assistance with the TEM characterization. We are grateful to two anonymous reviewers and Professor M. Matsui who provided us with very constructive comments that significantly improved our paper. This investigation was financially supported by the Fundamental Research Funds for the Central Universities from the Administer of Education of P. R. China (to X. Liu) and the National Natural Science Foundation of China (Grant #41090371).

References

Biernacki L, Pokrzywnicki S (1999) The thermal decomposition of manganese carbonate. J Thermal Anal Calorim 55:227–232

Binns RA, Davis RJ, Reed SBJ (1969) Ringwoodite natural (Mg, Fe)$_2$SiO$_4$ spinel in Tenham meteorite. Nature 221:943–944

Catti M, Freyria Fava F, Zicovich C, Dovesi R (1999) High-pressure decomposition of MCr_2O_4 spinels (M = Mg, Mn, Zn) by ab initio methods. Phys Chem Miner 26:389–395

Della Giusta A, Ottonello G (1993) Energy and long-range disorder in simple spinels. Phys Chem Miner 20:228–241

Dick HJB, Bullen T (1984) Chromian spinel as a petrogenetic indicator in abyssal and alpine-type peridotites and spatially associated lavas. Contrib Miner Petrol 86:54–76

Fei Y (1995) Thermal expansion. In: Ahrens TJ (eds) Mineral physics and crystallography: a handbook of physical constants. American Geophysical Union, Washington, DC, Shelf 2, pp 29–44

Fiorani D, Viticoli S (1980) Investigations on magnetically dilute $Co_xZn_{1-x}Rh_2O_4$ spinel solid solutions. J Phys Chem Solids 41:1041–1045

Freyria Fava F, Baraille I, Lichanot A, Larrieu C, Dovesi R (1997) On the structural, electronic and magnetic properties of $MnCr_2O_4$ spinel. J Phys: Condens Matter 9:10715–10724

Gilewicz-Wolter J, Zurek Z, Dudala J, Lis J, Homa M, Wolter M (2005) Diffusion of chromium, manganese, and iron in $MnCr_2O_4$ spinel. J Phase Equilib Diff 26:561–564

Grimes NW, Al-Ajaj EA (1992) Low-temperature thermal expansion of spinel. J Phys: Condens Matter 4:6375–6380

Gross J, Treiman AH (2011) Unique spinel-rich lithology in lunar meteorite ALHA81005: origin and possible connection to M3 observations of the farside highlands. J Geophys Res 116: E10009

Harrison RJ, Redfern SAT, HStC O'Neill (1998) The temperature dependence of the cation distribution in synthetic hercynite ($FeAl_2O_4$) from in situ neutron structure refinements. Am Miner 83:1092–1099

Hastings JM, Corliss LM (1962) Magnetic structure of manganese chromite. Phys Rev 126:556–565

Hazen RM, Yang H (1999) Effect of cation substitution and order-disorder on P-V-T equations of state of cubic spinels. Am Miner 84:1956–1960

He Q, Liu X, Hu X, Li S, Wang H (2011) Solid solution between lead fluorapatite and lead fluorvanadate apatite: mixing behavior, Raman feature and thermal expansivity. Phys Chem Miner 38:741–752

Hill RJ, Craig JR, Gibbs GV (1979) Systematics of the spinel structure type. Phys Chem Miner 4:317–339

Hu X, Liu X, He Q, Wang H, Qin S, Ren L, Wu C, Chang L (2011) Thermal expansion of andalusite and sillimanite at ambient pressure: a powder X-ray diffraction study up to 1,000°C. Miner Mag 75:363–374

Inoue T, Tanimoto Y, Irifune T, Suzuki T, Fukui H, Ohtaka O (2004) Thermal expansion of wadsleyite, ringwoodite, hydrous wadsleyite and hydrous ringwoodite. Phys Earth Planet Inter 143–144:279–290

Jacob KT, Fitzner K (1977) Ion-exchange equilibria between (Mn, Co)O solid solution and (Mn, Co)Cr_2O_4 and (Mn, Co)Al_2O_4 spinel solid solutions at 1100°C. J Mater Sci 12:481–488

Jacob KT, Patil R (1998) Activities in the spinel solid solution $Fe_xMg_{1-x}Al_2O_4$. Metall Mater Trans B29:1241–1248

Jung IH (2006) Critical evaluation and thermodynamic modeling of the Mn–Cr–O system for the oxidation of SOFC interconnect. Solid State Ionics 177:765–777

Klemme S, Ahrens M (2007) Low-temperature heat capacities of $MgAl_2O_4$ and spinels of the $MgCr_2O_4$-$MgAl_2O_4$ solid solution. Phys Chem Miner 34:59–72

Kovtunenko PV (1997) Defect formation in spinels in oxygen nonstoichiometry (a review). Glass Ceram 54:143–148

Lenaz D, Skogby H, Princivalle F, Hålenius U (2004) Structural changes and valence states in the $MgCr_2O_4$-$FeCr_2O_4$ solid solution series. Phys Chem Miner 31:633–642

Lenaz D, Skogby H, Princivalle F, Hålenius U (2006) The $MgCr_2O_4$-$MgFe_2O_4$ solid solution series: effects of octahedrally coordinated Fe^{3+} on T-O bond lengths. Phys Chem Miner 33:465–474

Levy D, Artioli G (1998) Thermal expansion of chromites and zinc spinels. Mater Sci Forum 278–281:390–395

Levy D, Diella V, Dapiaggi M, Sani A, Gemmi M, Pavese A (2004) Equation of state, structural behavior and phase diagram of synthetic $MgFe_2O_4$, as a function of pressure and temperature. Phys Chem Miner 31:122–129

Levy D, Diella V, Pavese A, Dapiaggi M, Sani A (2005) P-V equation of state, thermal expansion, and P-T stability of synthetic zincochromite ($ZnCr_2O_4$ spinel). Am Miner 90:1157–1162

Liu X, Prewitt CT (1990) High-temperature x-ray diffraction study of Co_3O_4: transition from normal to disordered spinel. Phys Chem Miner 17:168–172

Liu L, Zhang J, Green HW II, Jin Z, Bozhilov KN (2007) Evidence of former stishovite in metamorphosed sediments, implying subduction to > 350 km. Earth Planet Sci Lett 263:180–191

Liu X, Wang S, He Q, Chen J, Wang H, Li S, Peng F, Zhang L, Fei Y (2012) Thermal elastic behavior of $CaSiO_3$-walstromite: a powder X-ray diffraction study up to 900°C. Am Miner (in press). doi:10.2138/am.2012.3689

Moriwake H, Tanaka I, Oba F, Koyama Y, Adachi H (2002) Formation energy of Cr/Al vacancies in spinel $MgCr_2O_4$ and $MgAl_2O_4$ by first-principles calculations. Phys Rev B65: 153103

O'Neill HStC, Dollase WA (1994) Crystal structures and cation distributions in simple spinels from powder XRD structural refinements: $MgCr_2O_4$, $ZnCr_2O_4$, Fe_3O_4 and the temperature dependence of the cation distribution in $ZnAl_2O_4$. Phys Chem Miner 20:541–555

O'Neill HStC, Navrotsky A (1983) Simple spinels: crystallographic parameters, cation radii, lattice energies, and cation distribution. Am Miner 68:181–194

O'Neill HStC, Navrotsky A (1984) Cation distribution and thermodynamic properties of binary spinel solid solutions. Am Miner 69:733–753

O'Neill HStC, Redfern SAT, Kesson S, Short S (2003) An in situ neutron diffraction study of cation disordering in synthetic qandilite Mg_2TiO_4 at high temperatures. Am Miner 88:860–865

Paraskevopoulos GM, Economou M (1981) Zoned Mn-rich chromite from podiform type chromite ore in serpentinites of northern Greece. Am Miner 66:1013–1019

Park JH, Jung I-H, Lee S-B (2009) Phase diagram study for the CaO-SiO_2-Cr_2O_3–5 mass. % MgO-10mass. % MnO system. Met Mater Int 15:677–681

Pieters CM, Besse S, Boardman J, Buratti B, Cheek L, Clark RN, Combe JP, Dhingra D, Goswami JN, Green RO, Head JW, Isaacson P, Klima R, Kramer G, Lundeen S, Malaret E, McCord T, Mustard J, Nettles J, Petro N, Runyon C, Staid M, Sunshine J, Taylor LA, Thaisen K, Tompkins S, Whitten J (2011) Mg-spinel lithology: a new rock-type on the lunar farside. J Geophys Res 116:E00G08

Qu W, Jian L, Hill JM, Ivey DG (2006) Electrical and microstructural characterization of spinel phases as potential coatings for SOFC metallic interconnects. J Power Sources 153:114–124

Raccah PM, Bouchard RJ, Wold A (1966) Crystallographic study of chromium spinels. J Appl Phys 37:1436–1437

Rosén E, Muan A (1966) Stability of $MgAl_2O_4$ at 1400°C as derived from equilibrium measurements in $CoAl_2O_4$-$MgAl_2O_4$ solid solutions. J Am Ceram Soc 49:107–108

Ross NL, Navrotsky (1987) The Mg_2GeO_4 olivine-spinel phase transition. Phys Chem Miner 14:473–481

Shannon RD (1976) Revised effective ionic radii and systematic studies of interatomic distances in halides and chalcogenides. Acta Cryst A32:751–767

Skinner BJ (1966) Thermal expansion. In: Clark SP (eds) Handbook of physical constants. Geol Soc Am Mem, pp 75–95

Smyth JR, Jacobsen SD, Hazen RM (2000) Comparative crystal chemistry of orthosilicate minerals. In: Hazen RM, Downs RT (eds) High-temperature and high-pressure crystal chemistry. Reviews in mineralogy and geochemistry, vol 41. Mineralogical Society of American, Washington, DC, pp 187–209

Song SH, Yuan ZX, Xiao P (2003) Electrical properties of $MnCr_2O_4$ spinel. J Mater Sci Lett 22:755–757

Stefan E, Irvine JTS (2011) Synthesis and characterization of chromium spinels as potential electrode support materials for intermediate temperature solid oxide fuel cells. J Mater Sci 46:7191–7197

Suzuki I, Kumazawa M (1980) Anomalous thermal expansion in spinel $MgAl_2O_4$. Phys Chem Miner 5:279–284

Yamanaka T (1986) Crystal structures of Ni_2SiO_4 and Fe_2SiO_4 as a function of temperature and heating duration. Phys Chem Miner 13:227–232

Yamanaka T, Takéuchi Y (1983) Order-disorder transition in $MgAl_2O_4$ spinel at high temperatures up to 1700°C. Z Kristallogr 165:65–78